Electronic Supplementary Material (ESI) for Journal of Materials Chemistry A.


# Structure-property insights into nanostructured electrodes for Li-ion batteries from local structural and diffusional probes

**Josefa Vidal Laveda,[a] Beth Johnston, [a] Gary W. Paterson,[b] Peter J. Baker,[c] Matthew G. Tucker,[d] Helen Y. Playford,[c] Kirsten M. Ø. Jensen,[e] Simon J. L. Billinge[e,f] and Serena A. Corr[*a]**

[a]*School of Chemistry, University of Glasgow, Glasgow, G12 8QQ, UK. E-mail: serena.corr@glasgow.ac.uk; Tel: +44 (0)141 3302274*

[b]*School of Physics and Astronomy, University of Glasgow, Glasgow, G12 8QQ, UK.*

[c]*ISIS Pulsed Neutron and Muon Source, STFC Rutherford Appleton Laboratory, Harwell Science and Innovation Campus, Didcot, Oxfordshire OX11 0QX, UK*

[d]*Spallation Neutron Source, Oak Ridge National Laboratory, Oak Ridge, Tennessee, 37831, USA*

[e]*Department of Applied Physics and Applied Mathematics, Columbia University, New York, New York 10027, USA*

[f]*Condensed Matter Physics and Materials Science, Department Brookhaven National Laboratory, Upton, New York 11973, USA*

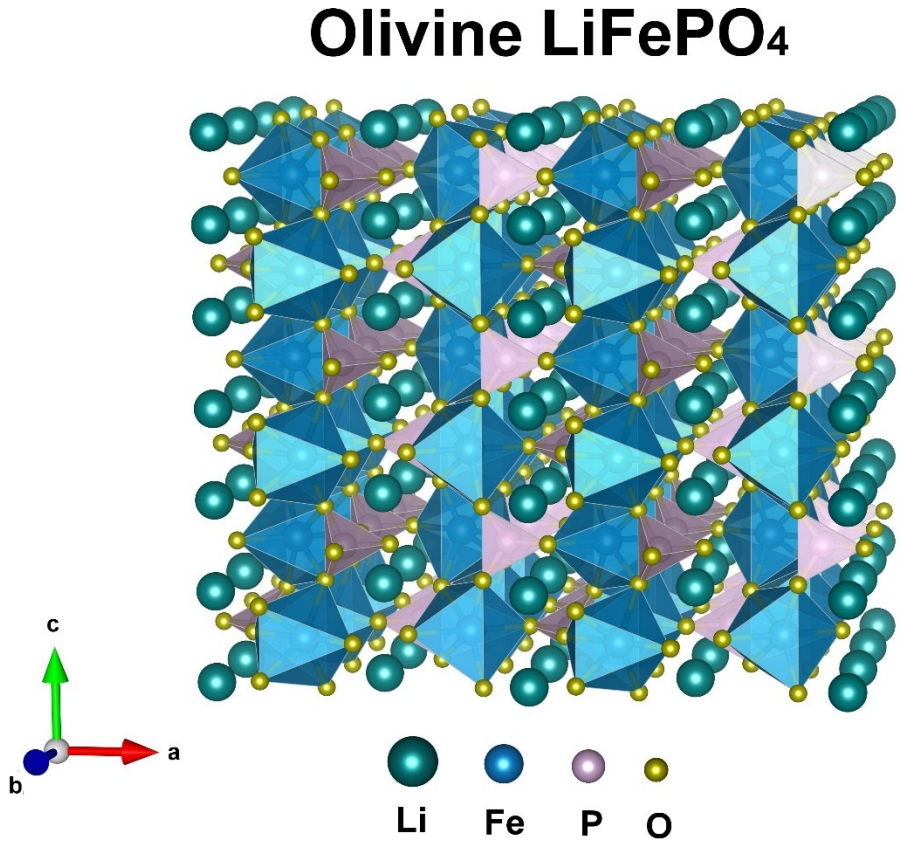


**Figure S1.** Crystal structure of olivine $LiFePO_4$.

**Table S1.** List of precursor for the microwave synthesis of $LiFe_{1-x}Mn_xPO_4$ olivines.

| Samples | Reactants |
|---|---|
| **$LiFePO_4$** | $Fe(acac)_3$ (0.7063 g, 2 mmol)+$LiH_2PO_4$ (0.2079 g, 2 mmol) + 10 mL EG |
| **$LiFe_{0.75}Mn_{0.25}PO_4$** | $Fe(acac)_3$ (0.5298 g, 1.5 mmol)+$MnC_2O_4{\cdot}2H_2O$ (0.0895 g, 0.5 mmol)+$LiH_2PO_4$ (0.2079 g, 2 mmol) + 10 mL EG |
| **$LiFe_{0.5}Mn_{0.5}PO_4$** | $Fe(acac)_3$ (0.3532 g, 1 mmol)+$MnC_2O_4{\cdot}2H_2O$ (0.1790 g, 1 mmol)+$LiH_2PO_4$ (0.2079 g, 2 mmol) + 10 mL EG |
| **$LiFe_{0.25}Mn_{0.75}PO_4$** | $Fe(acac)_3$ (0.1766 g, 0.5 mmol)+$MnC_2O_4{\cdot}2H_2O$ (0.2685 g, 1.5 mmol)+$LiH_2PO_4$ (0.2079 g, 2 mmol) + 10 mL EG |
| **$LiMnPO_4$** | $Mn(acac)_3$ (0.7045 g, 2 mmol)+$LiH_2PO_4$ (0.2079 g, 2 mmol) + 10 mL EG |

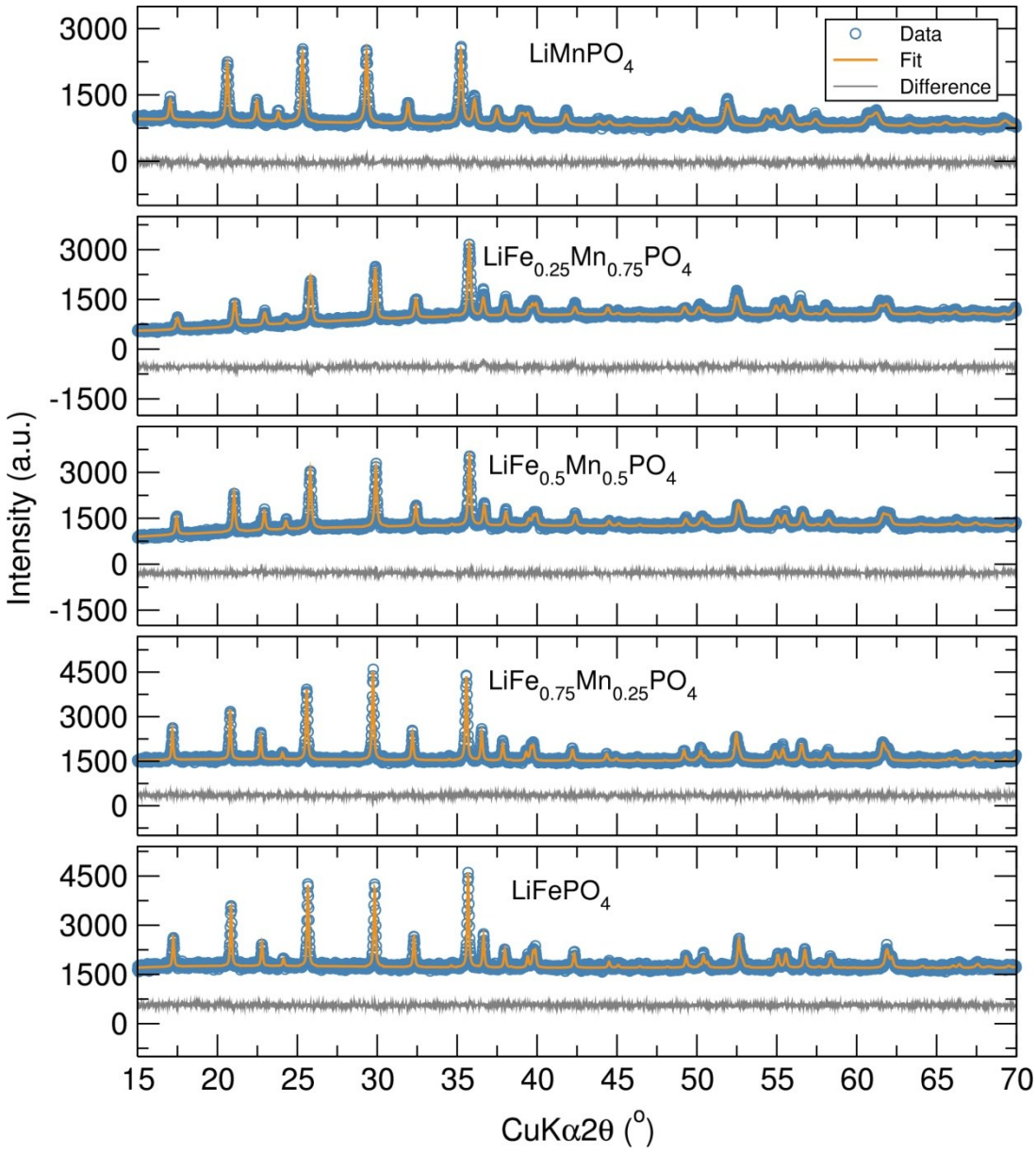


**Figure S2.** Rietveld analysis of PXRD data from $LiFe_{1-x}Mn_xPO_4$ ($x$ = 0, 0.25, 0.5, 0.75, 1) olivines to an orthorhombic *Pnma* structure. Dots represent observed data and solid line the calculated pattern. The lower line is the difference curve.

**Table S2.** Calculated lattice parameters for the $LiFe_{1-x}Mn_xPO_4$ olivines obtained from Rietveld refinements of PXRD data.

| **Sample** | **$LiFePO_4$** | **$LiFe_{0.75}Mn_{0.25}PO_4$** | **$LiFe_{0.5}Mn_{0.5}PO_4$** | **$LiFe_{0.25}Mn_{0.75}PO_4$** | **$LiMnPO_4$** |
|---|---|---|---|---|---|
| Space group | *Pnma* | *Pnma* | *Pnma* | *Pnma* | *Pnma* |
| *a* (Å) | 10.3303(5) | 10.3628(5) | 10.3899(7) | 10.4213(9) | 10.4504(8) |
| *b* (Å) | 6.0000(3) | 6.0200(3) | 6.0460(4) | 6.0761(5) | 6.1043(5) |
| *c* (Å) | 4.6948(3) | 4.7052(3) | 4.7197(4) | 4.7344(5) | 4.7471(5) |
| *V* ($Å^{-3}$) | 291.00(4) | 293.53(4) | 296.48(5) | 299.78(7) | 302.83(7) |
| $R_{wp}$ | 0.0254 | 0.0272 | 0.0328 | 0.0400 | 0.0373 |
| $R_p$ | 0.0202 | 0.0218 | 0.0260 | 0.0316 | 0.0298 |
| $X^2$ | 1.164 | 1.196 | 1.360 | 1.577 | 1.293 |

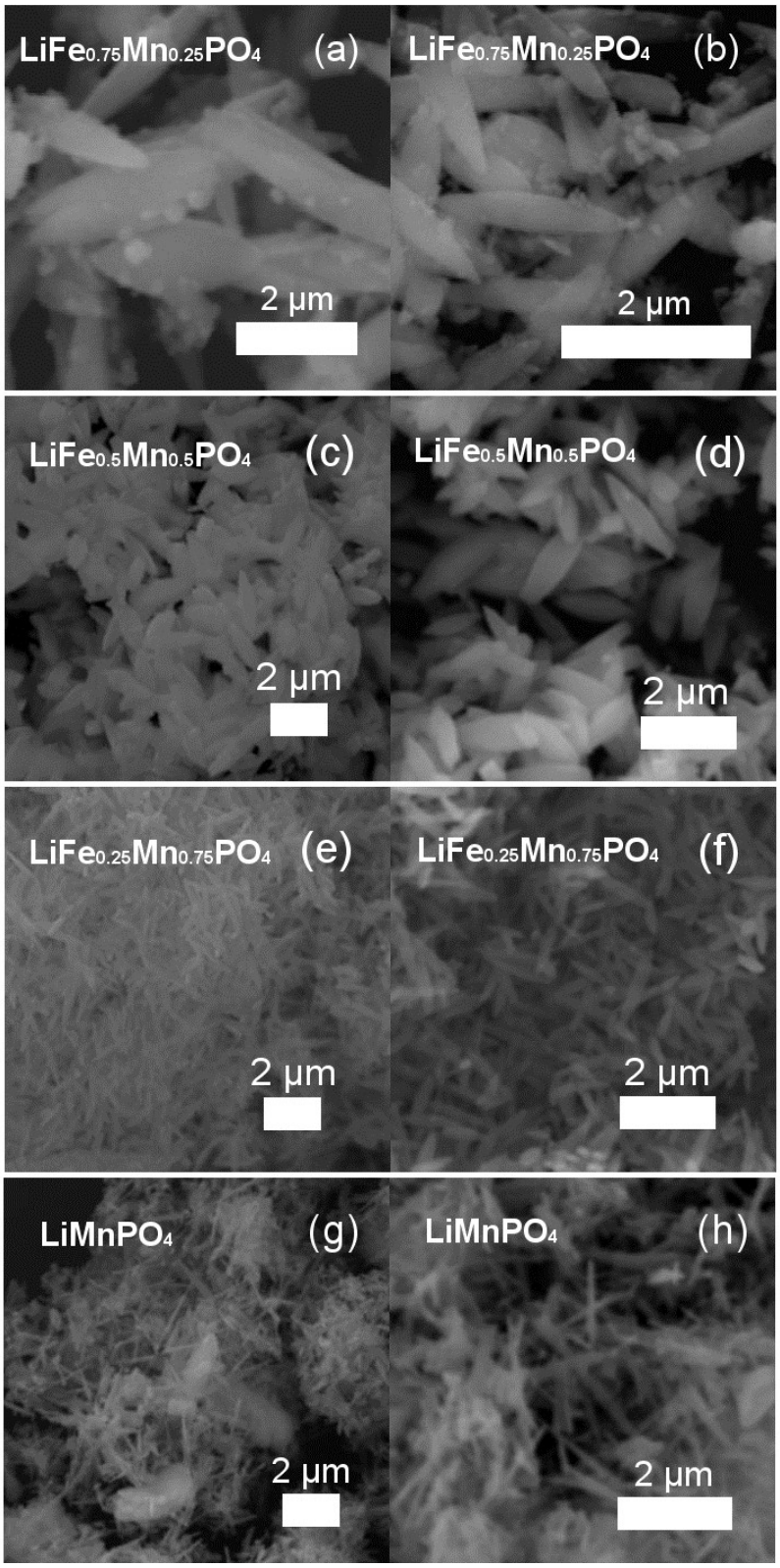


**Figure S3.** SEM images of $LiFe_{1-x}Mn_xPO_4$ ($x$= 0.25, 0.5, 0.75, 1) powders. **(a, b)** $LiFe_{0.75}Mn_{0.25}PO_4$. **(c, d)** $LiFe_{0.5}Mn_{0.5}PO_4$. **(e, f)** $LiFe_{0.25}Mn_{0.75}PO_4$. **(g, h)** $LiMnPO_4$.

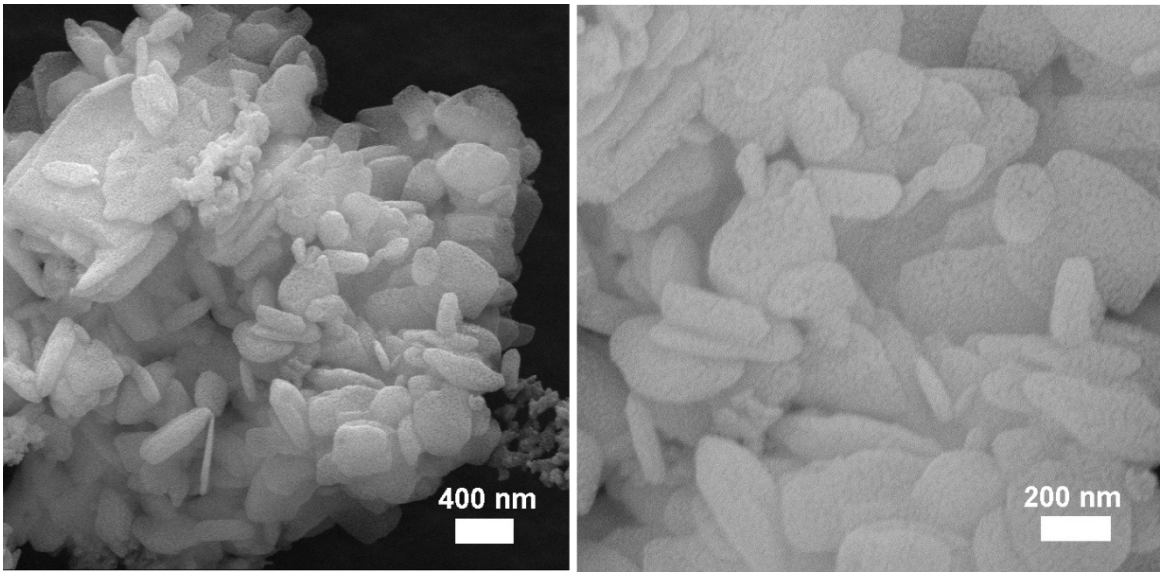


**Figure S4.** SEM images of $LiFePO_4$ particles.

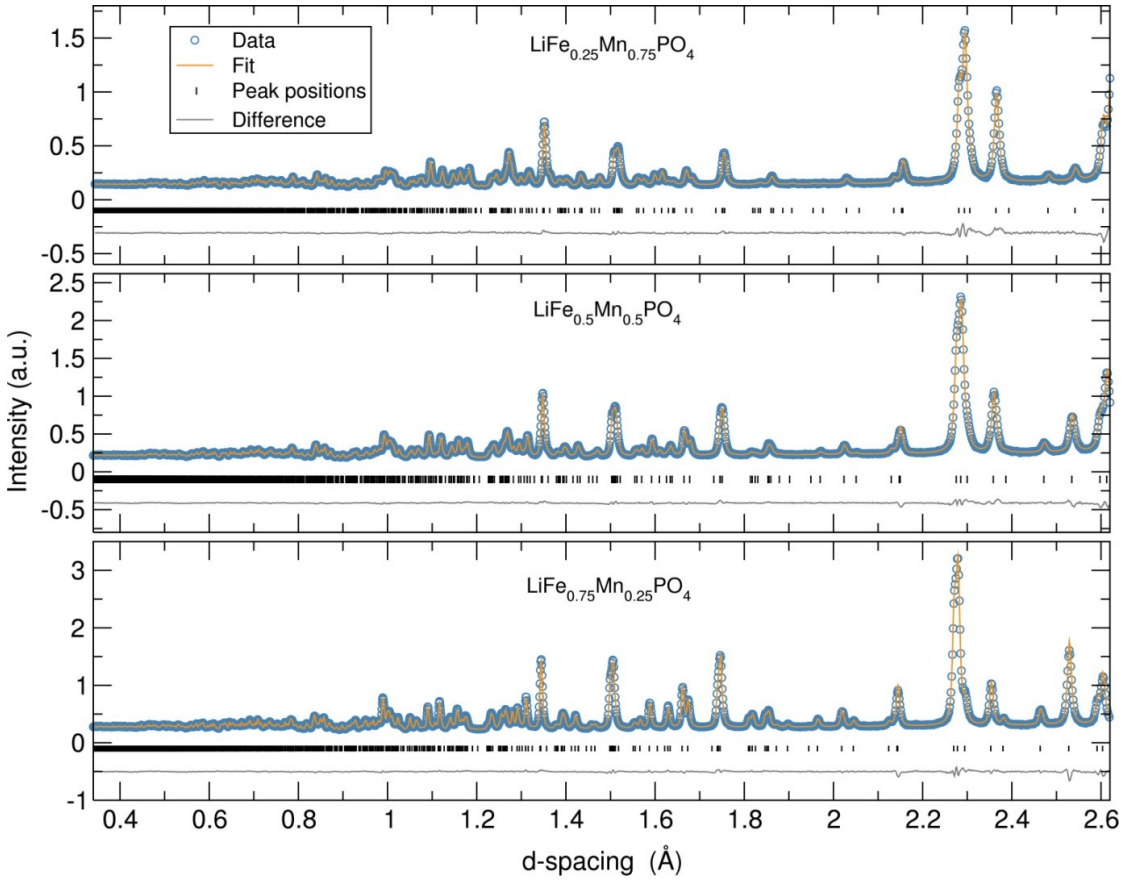


**Figure S5.** Rietveld refinements of high resolution PND data of mixed metal phosphates $LiFe_{1-x}Mn_xPO_4$ ($x$= 0.25, 0.5 and 0.75) nanostructures (detector bank 5). Dots represent observed data and solid line the calculated pattern. The lower line is the difference curve.

**Table S3.** Structural parameters of $LiFePO_4$ sample from Rietveld analysis of high resolution PND data at room temperature.

| **$LiFePO_4$** | | $R_{exp}$=0.0193 | $R_{wp}$=0.0153 | $\chi^2$=1.879 | *d*=3.564 mg/cm$^3$ | |
|---|---|---|---|---|---|---|
| *Pnma* | | *a*=10.3386(2) Å | *b*=0.0003(1) Å | *c*=4.6947(1) Å | *V*=291.24(1) Å$^3$ | |
| Atom | Site | *x* | *y* | *z* | Uiso (Å$^2$) | Frac |
| $^7$Li | 4*a* | 0.0000 | 0.0000 | 0.0000 | 0.015(1) | 0.747(7) |
| Fe | 4*c* | 0.2819(1) | 0.2500 | 0.9752(1) | 0.0049(1) | 1.001(2) |
| P | 4*c* | 0.0954(1) | 0.2500 | 0.4182(1) | 0.0029(1) | 1.000 |
| O | 4*c* | 0.0977(1) | 0.2500 | 0.7420(2) | 0.0068(1) | 1.000 |
| O | 4*c* | 0.4575(1) | 0.2500 | 0.2057(2) | 0.0066(1) | 1.000 |
| O | 8*d* | 0.1658(1) | 0.0474(1) | 0.2854(1) | 0.0062(1) | 1.000 |
| $^6$Li | 4*a* | 0.0000 | 0.0000 | 0.0000 | 0.015(1) | 0.030 |

**Table S4.** Structural parameters of $LiFe_{0.75}Mn_{0.25}PO_4$ sample from the Rietveld analysis of high resolution powder neutron diffraction data at room temperature.

| **$LiFe_{0.75}Mn_{0.25}PO_4$** | | $R_{exp}$=0.0174 | $R_{wp}$=0.0144 | $\chi^2$=1.879 | *d*=3.538 mg/cm$^3$ | |
|---|---|---|---|---|---|---|
| *Pnma* | | *a*=10.3646(2) Å | *b*=6.0222(1) Å | *c*=4.7055(1) Å | *V*=293.71(2) Å$^3$ | |
| Atom | Site | *x* | *y* | *z* | Uiso (Å$^2$) | Frac |
| $^7$Li | 4*a* | 0.0000 | 0.0000 | 0.0000 | 0.013(1) | 0.807(7) |
| Fe | 4*c* | 0.2820(1) | 0.2500 | 0.9735(1) | 0.0052(1) | 0.771(1) |
| Mn | 4*c* | 0.2820(1) | 0.2500 | 0.9735(1) | 0.0052(1) | 0.229(1) |
| P | 4*c* | 0.0949(1) | 0.2500 | 0.4158(1) | 0.0029(1) | 1.000 |
| O | 4*c* | 0.0975(1) | 0.2500 | 0.7393(2) | 0.0067(1) | 1.000 |
| O | 4*c* | 0.4571(1) | 0.2500 | 0.2073(2) | 0.0071(1) | 1.000 |
| O | 8*d* | 0.1651(1) | 0.0479(1) | 0.2839(1) | 0.0066(1) | 1.000 |
| $^6$Li | 4*a* | 0.0000 | 0.0000 | 0.0000 | 0.013(1) | 0.030 |

**Table S5.** Structural parameters of $LiFe_{0.5}Mn_{0.5}PO_4$ sample from Rietveld analysis of high resolution PND data at room temperature.

| **$LiFe_{0.5}Mn_{0.5}PO_4$** | $R_{exp}$=0.0176 | $R_{wp}$=0.0150 | $\chi^2$=1.879 | *d*=3.511 mg/cm$^3$ |
|---|---|---|---|---|
| *Pnma* | *a*=10.3901(3) Å | *b*=6.0454(2) Å | *c*=4.7167(1) Å | *V*=296.27(2) Å$^3$ |

| Atom | Site | *x* | *y* | *z* | Uiso (Å$^2$) | Frac |
|---|---|---|---|---|---|---|
| $^7$Li | 4*a* | 0.0000 | 0.0000 | 0.0000 | 0.011(1) | 0.858(8) |
| Fe | 4*c* | 0.2821(1) | 0.2500 | 0.9714(3) | 0.0070(3) | 0.521(1) |
| Mn | 4*c* | 0.2821(1) | 0.2500 | 0.9714(3) | 0.0070(3) | 0.479(1) |
| P | 4*c* | 0.0945(1) | 0.2500 | 0.4129(2) | 0.0025(1) | 1.000 |
| O | 4*c* | 0.0973(1) | 0.2500 | 0.7355(2) | 0.0066(1) | 1.000 |
| O | 4*c* | 0.4567(1) | 0.2500 | 0.2091(2) | 0.0076(1) | 1.000 |
| O | 8*d* | 0.1640(1) | 0.0487(1) | 0.2820(1) | 0.0068(1) | 1.000 |
| $^6$Li | 4*a* | 0.0000 | 0.0000 | 0.0000 | 0.011(1) | 0.030 |

**Table S6.** Structural parameters of $LiFe_{0.25}Mn_{0.75}PO_4$ sample from Rietveld analysis of high resolution PND data at room temperature.

| **$LiFe_{0.25}Mn_{0.75}PO_4$** | $R_{exp}$=0.0234 | $R_{wp}$=0.0169 | $\chi^2$=1.879 | *d*=3.476 mg/cm$^3$ |
|---|---|---|---|---|
| *Pnma* | *a*=10.4168(2) Å | *b*=6.0713(1) Å | *c*=4.7287(1) Å | *V*=299.06(3) Å$^3$ |

| Atom | Site | *x* | *y* | *z* | Uiso (Å$^2$) | Frac |
|---|---|---|---|---|---|---|
| $^7$Li | 4*a* | 0.0000 | 0.0000 | 0.0000 | 0.010(1) | 0.883(8) |
| Fe | 4*c* | 0.280(1) | 0.2500 | 0.977(3) | 0.007 | 0.249(1) |
| Mn | 4*c* | 0.280(1) | 0.2500 | 0.977(3) | 0.007 | 0.751(1) |
| P | 4*c* | 0.0937(1) | 0.2500 | 0.4103(2) | 0.0029(1) | 1.000 |
| O | 4*c* | 0.0976(1) | 0.2500 | 0.7317(2) | 0.0068(1) | 1.000 |
| O | 4*c* | 0.4561(1) | 0.2500 | 0.2106(2) | 0.0066(1) | 1.000 |
| O | 8*d* | 0.1629(1) | 0.0497(1) | 0.2796(1) | 0.0062(1) | 1.000 |
| $^6$Li | 4*a* | 0.0000 | 0.0000 | 0.0000 | 0.010(1) | 0.030 |

**Table S7.** Structural parameters of $LiMnPO_4$ sample from Rietveld analysis of high resolution PND data at room temperature.

| **$LiMnPO_4$** | $R_{exp}$=0.0287 | $R_{wp}$=0.0205 | $\chi^2$=1.879 | *d*=3.496 mg/cm$^3$ |
|---|---|---|---|---|
| *Pnma* | *a*=10.4470(5) Å | *b*=6.1012(3) Å | *c*=4.7440(2) Å | *V*=302.38(4) Å$^3$ |

| Atom | Site | *x* | *y* | *z* | Uiso (Å$^2$) | Frac |
|---|---|---|---|---|---|---|
| Li | 4*a* | 0.0000 | 0.0000 | 0.0000 | 0.0087(8) | 0.98(1) |
| Mn | 4*c* | 0.2815(2) | 0.2500 | 0.9694(4) | 0.0037(3) | 1.045(7) |
| P | 4*c* | 0.0928(1) | 0.2500 | 0.4080(2) | 0.0014(1) | 1.000 |
| O | 4*c* | 0.0988(1) | 0.2500 | 0.7295(2) | 0.0072(2) | 1.000 |
| O | 4*c* | 0.4550(1) | 0.2500 | 0.2108(3) | 0.0064(2) | 1.000 |
| O | 8*d* | 0.1619(1) | 0.0510(1) | 0.2768(2) | 0.0053(1) | 1.000 |

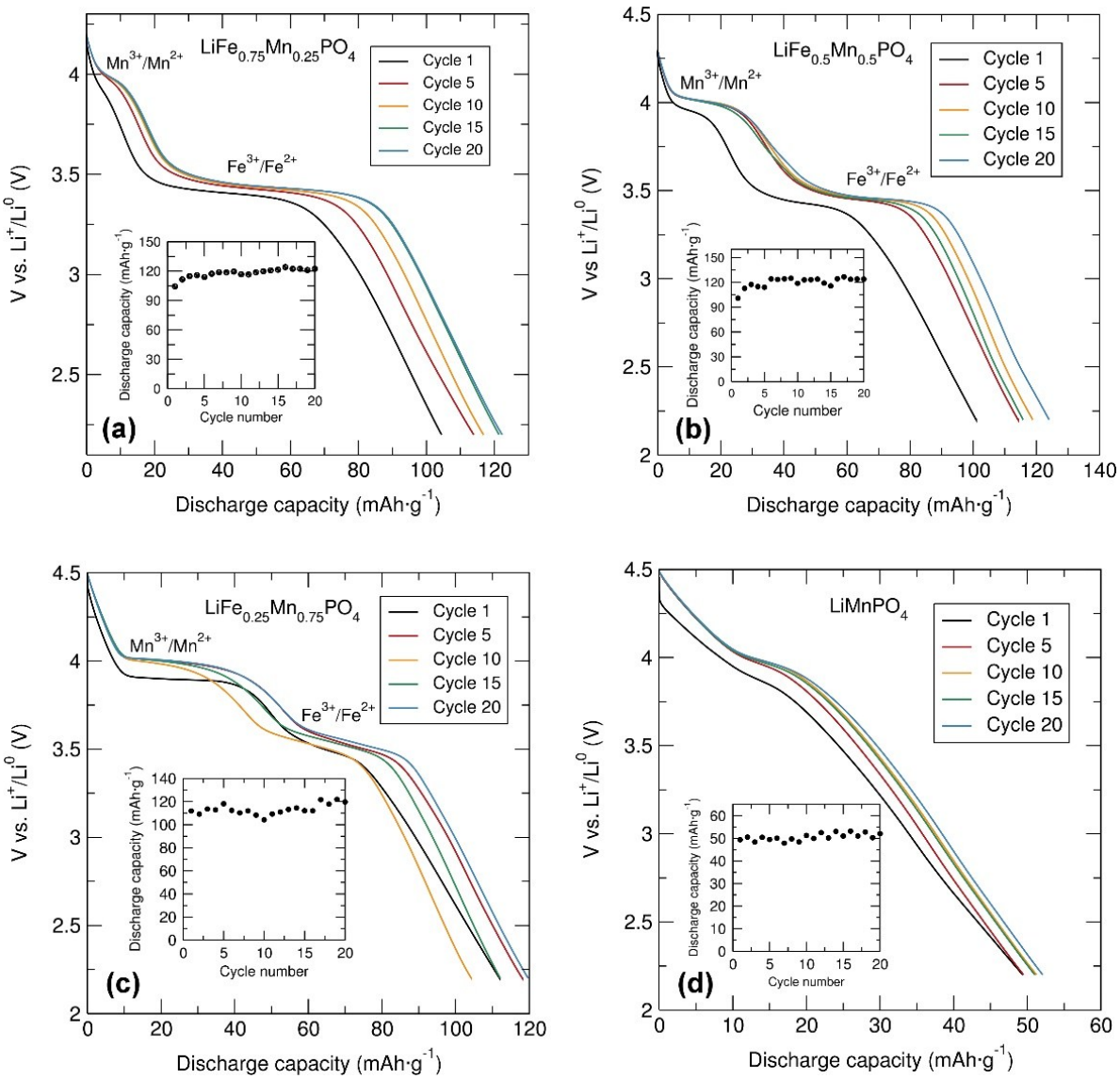


**Figure S6.** Cycling performance and cycling stability (inset) of C/LiFe$_{1-x}$Mn$_x$PO$_4$ (*x* = 0.25, 0.50, 0.75, 1) olivines coated with 15% wt. C from sucrose and mixed with C black and PTFE in 60:30:10 (% weight) between 2.2 V and 4.0, 4.2, 4.3 or 4.5 V (depending on Mn content) at C/20 rate.

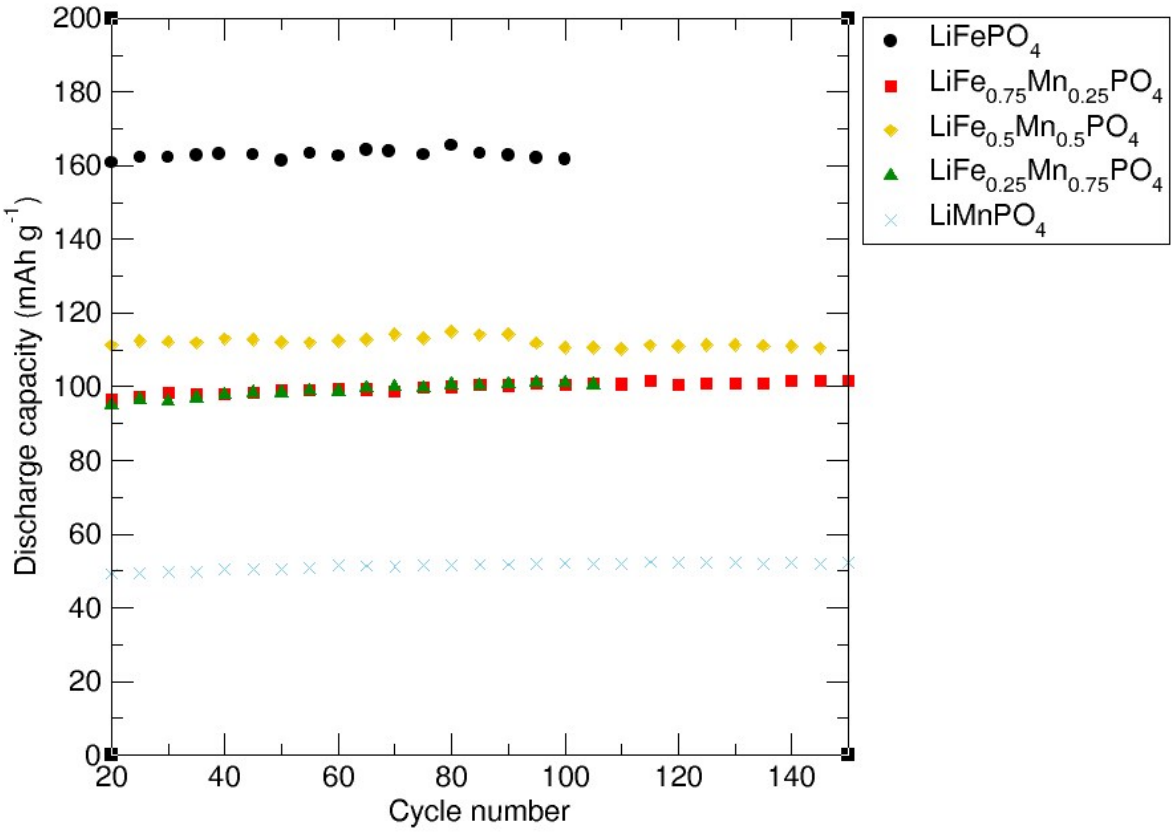


**Figure S7.** Extended cycling stability of C/$LiFe_{1-x}Mn_xPO_4$ ($x$ = 0.25, 0.50, 0.75, 1) olivines coated with 15% wt. C from sucrose and mixed with C black and PTFE in 60:30:10 (% weight) between 2.2 V and 4.0, 4.2, 4.3 or 4.5 V (depending on Mn content) at C/10 rate.

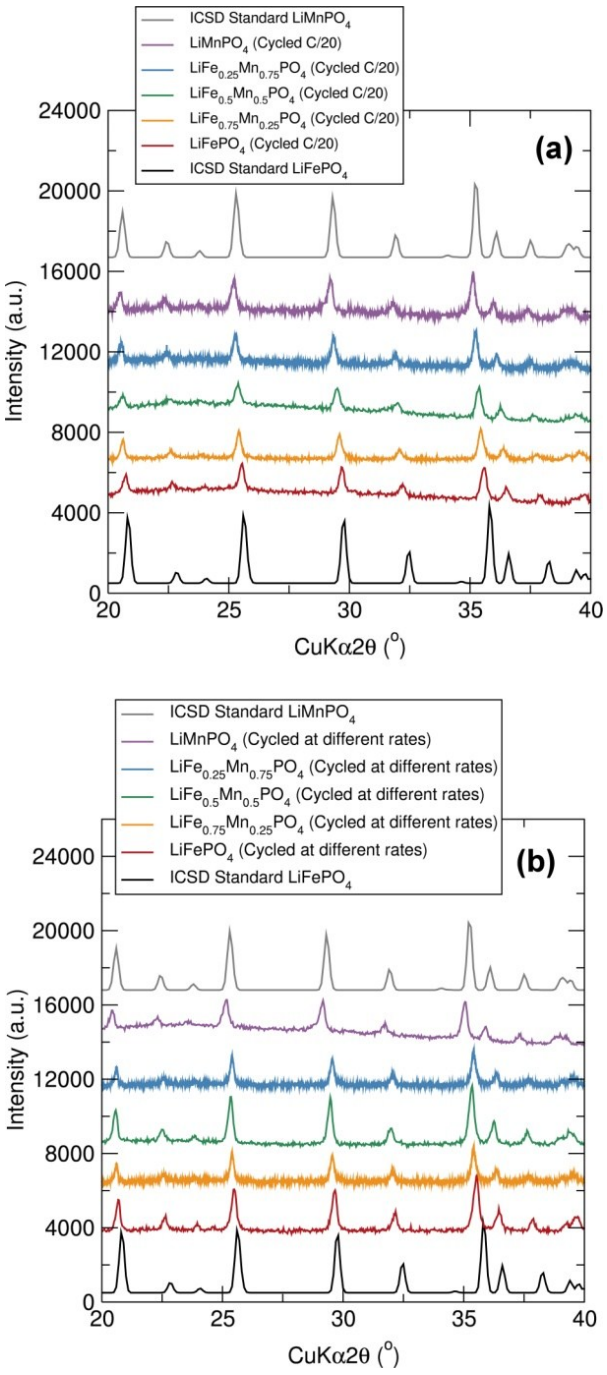


**Figure S8.** PXRD of post-cycled C/$LiFe_{1-x}Mn_xPO_4$ olivines in the discharged state after cycling at **(a)** C/20 for 20 cycles and **(b)** different charge-discharge rates.

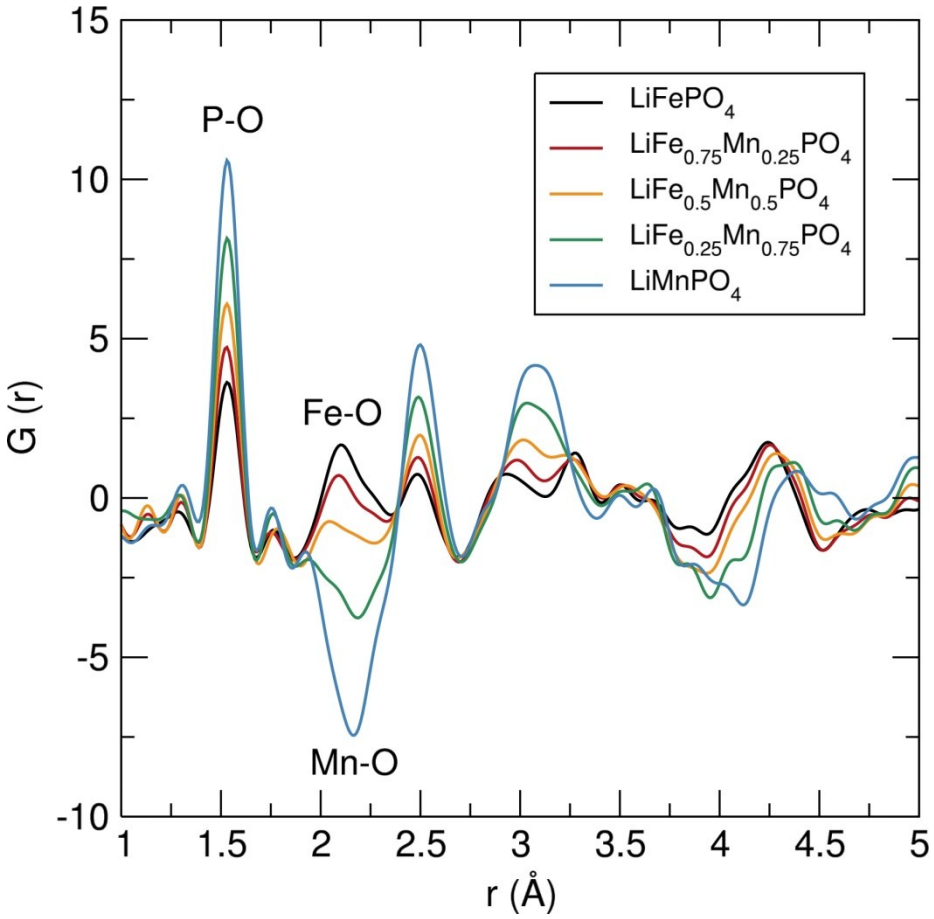


**Figure S9.** Raw neutron PDF data of $LiFe_{1-x}Mn_xPO_4$ ($x$ = 0, 0.25, 0.50, 0.75, 1) olivines from 1 to 5 Å at room temperature

**Table S8.** Calculated lattice parameters for the $LiFe_{1-x}Mn_xPO_4$ olivines obtained from real space Rietveld refinements of neutron PDF data from 1 to 30 Å.

| **Sample** | **$LiFePO_4$** | **$LiFe_{0.75}Mn_{0.25}PO_4$** | **$LiFe_{0.5}Mn_{0.5}PO_4$** | **$LiFe_{0.25}Mn_{0.75}PO_4$** | **$LiMnPO_4$** |
|---|---|---|---|---|---|
| Space group | *Pnma* | *Pnma* | *Pnma* | *Pnma* | *Pnma* |
| *a* (Å) | 10.356(8) | 10.386(7) | 10.407(3) | 10.435(6) | 10.468(5) |
| *b* (Å) | 6.017(6) | 6.037(5) | 6.056(5) | 6.084(4) | 6.114(3) |
| *c* (Å) | 4.701(4) | 4.713(3) | 4.726(4) | 4.736(3) | 4.753(2) |
| Scale factor | 0.70(4) | 0.69(3) | 0.70(3) | 0.73(2) | 0.68(2) |
| $R_{wp}$ | 0.1299 | 0.1331 | 0.1577 | 0.1468 | 0.1849 |

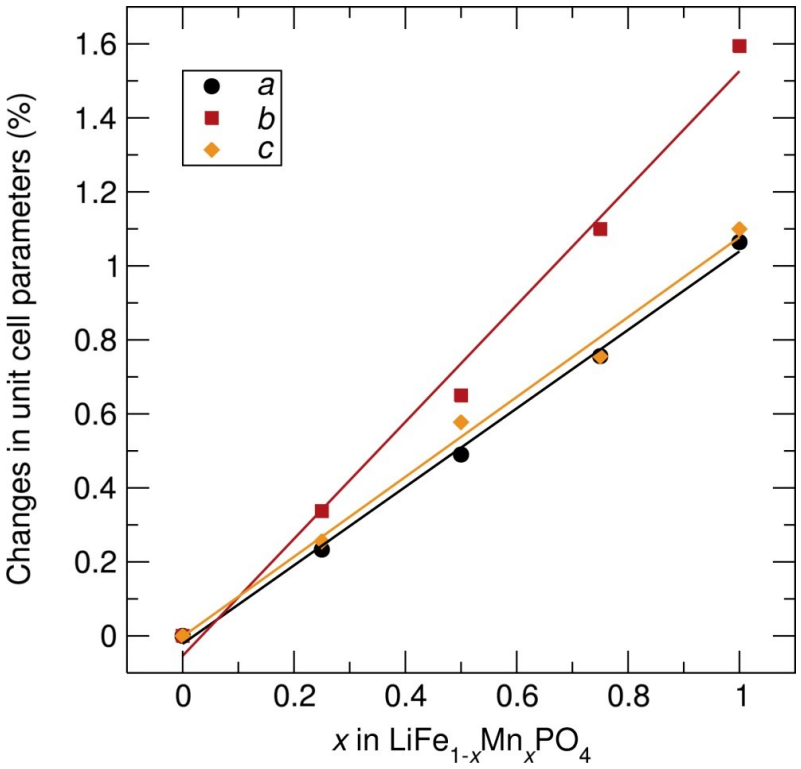


**Figure S10.** Changes in the unit-cell parameters as a function of the Mn content obtained from fitting neutron PDF data of the $LiFe_{1-x}Mn_xPO_4$ ($x$ = 0, 0.25, 0.50, 0.75, 1) olivines in the $r$ range from 1 to 30 Å.

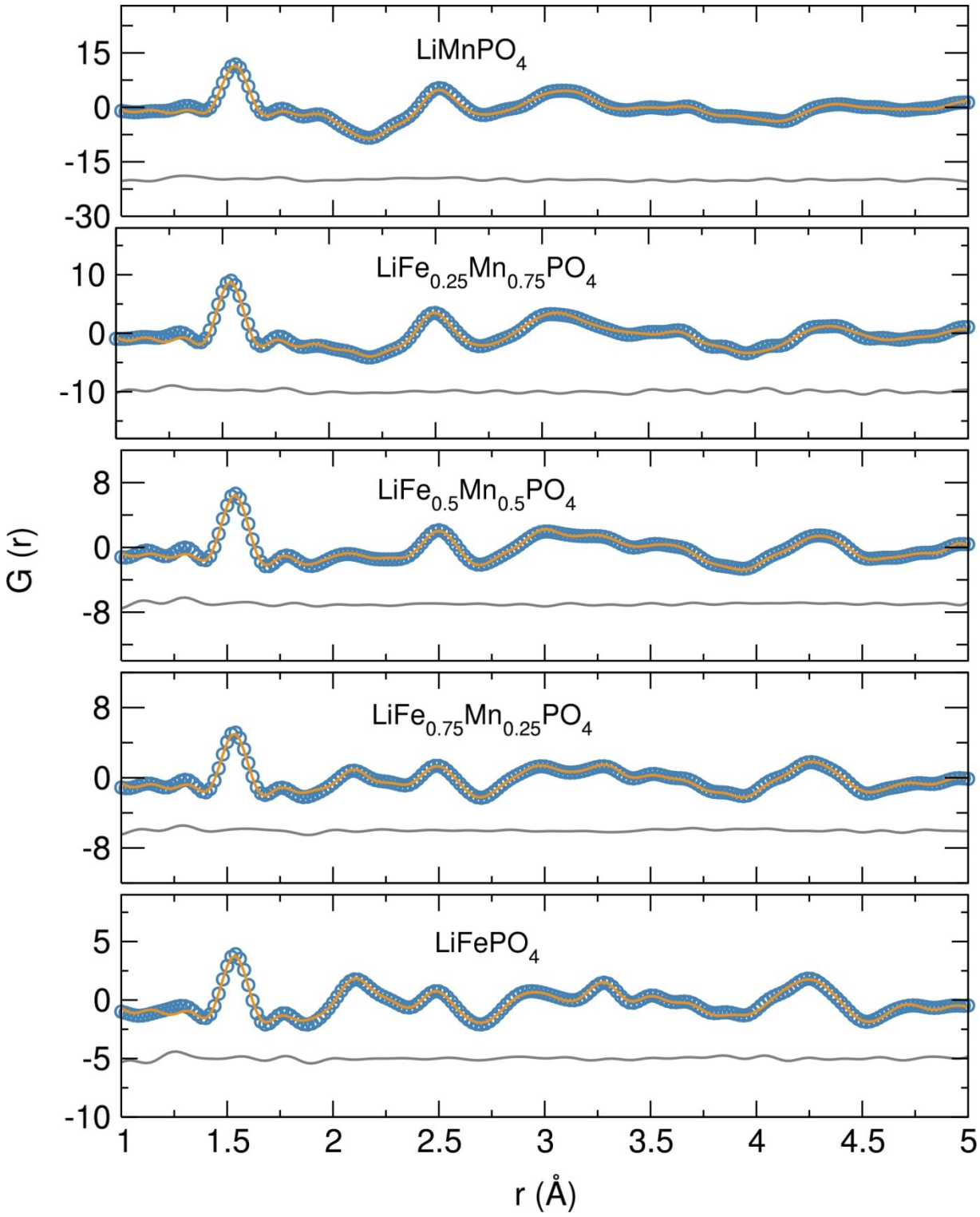


**Figure S11.** Fits of neutron PDF data obtained for single-phase $LiFe_{1-x}Mn_xPO_4$ (x = 0, 0.25, 0.5, 0.75, 1) olivines at room temperature in the *r* range from 1 Å to 5 Å. Dots represent observed data and solid line the calculated pattern. The lower line is the difference curve.

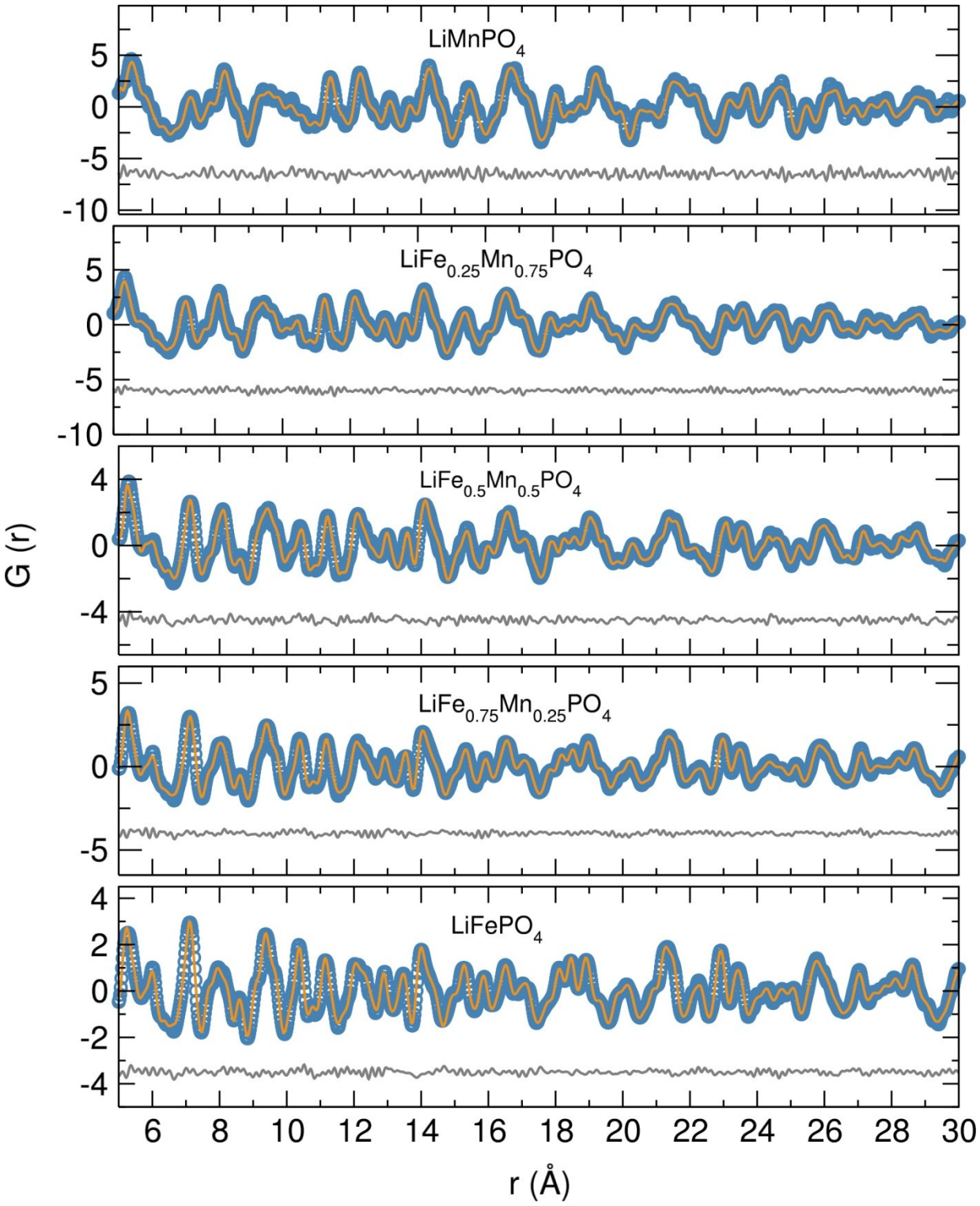


**Figure S12.** Fits of neutron PDF data obtained for single-phase $LiFe_{1-x}Mn_xPO_4$ (x = 0, 0.25, 0.5, 0.75, 1) olivines at room temperature in the *r* range from 5 Å to 30 Å. Dots represent observed data and solid line the calculated pattern. The lower line is the difference curve.

**Table S9.** $R_w$ values obtained from neutron PDF fits of $LiFe_{1-x}Mn_xPO_4$ ($x$ = 0, 0.25, 0.5, 0.75, 1) olivines at different $r$ ranges.

| $R_w$ | $LiFePO_4$ | $LiFe_{0.75}Mn_{0.25}PO_4$ | $LiFe_{0.5}Mn_{0.5}PO_4$ | $LiFe_{0.25}Mn_{0.75}PO_4$ | $LiMnPO_4$ |
|---|---|---|---|---|---|
| 1 - 5 Å | 0.1244 | 0.1211 | 0.1140 | 0.1289 | 0.1085 |
| 5 - 30 Å | 0.1074 | 0.1088 | 0.1336 | 0.1243 | 0.1776 |
| 1 - 30 Å | 0.1299 | 0.1331 | 0.1577 | 0.1468 | 0.1849 |

**Table S10.** Scale factor values obtained from neutron PDF fits of $LiFe_{1-x}Mn_xPO_4$ ($x$ = 0, 0.25, 0.5, 0.75, 1) olivines at different $r$ ranges.

| Scale factor | $LiFePO_4$ | $LiFe_{0.75}Mn_{0.25}PO_4$ | $LiFe_{0.5}Mn_{0.5}PO_4$ | $LiFe_{0.25}Mn_{0.75}PO_4$ | $LiMnPO_4$ |
|---|---|---|---|---|---|
| 1 - 5 Å | 0.76(8) | 0.68(9) | 0.72(7) | 0.75(3) | 0.82(2) |
| 5 - 30 Å | 0.69(5) | 0.68(2) | 0.69(3) | 0.70(4) | 0.66(3) |
| 1 - 30 Å | 0.70(4) | 0.68(3) | 0.70(3) | 0.73(2) | 0.68(2) |

**Table S11.** Calculated scale factor and amorphous content for the $LiFe_{1-x}Mn_xPO_4$ ($x$ = 0, 0.25, 0.5, 0.75, 1) olivines obtained from two isostructural phases refinements of neutron PDF data from 1 to 30 Å.

| Sample | $LiFePO_4$ | $LiFe_{0.75}Mn_{0.25}PO_4$ | $LiFe_{0.5}Mn_{0.5}PO_4$ | $LiFe_{0.25}Mn_{0.75}PO_4$ | $LiMnPO_4$ |
|---|---|---|---|---|---|
| Scale factor Phase 1 | 0.68(3) | 0.66(4) | 0.68(3) | 0.71(2) | 0.66(2) |
| Scale factor Phase 2 | 0.05(7) | 0.04(6) | 0.05(6) | 0.06(5) | 0.06(3) |
| Amorphous content (%) | 6.7 | 5.6 | 6.9 | 7.7 | 8.1 |
| *Spdiameter* (Å) | 15 | 18 | 14 | 12 | 12 |
| $R_{wp}$ | 0.1284 | 0.1321 | 0.1560 | 0.1446 | 0.1825 |

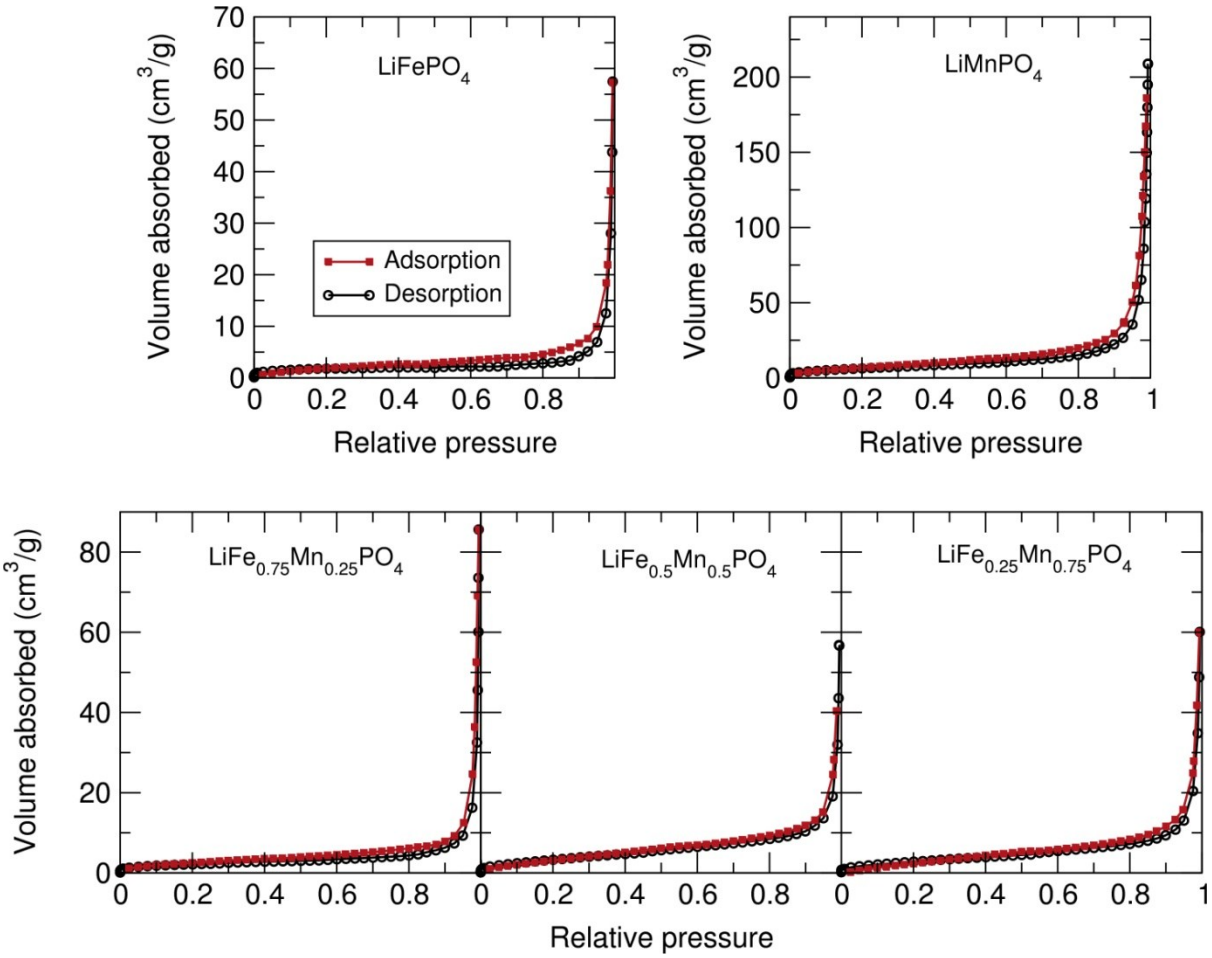


**Figure S13.** $N_2$ sorption isotherms at 77 K for $LiFe_{1-x}Mn_xPO_4$ ($x$ = 0, 0.25, 0.5, 0.75 and 1) olivines.

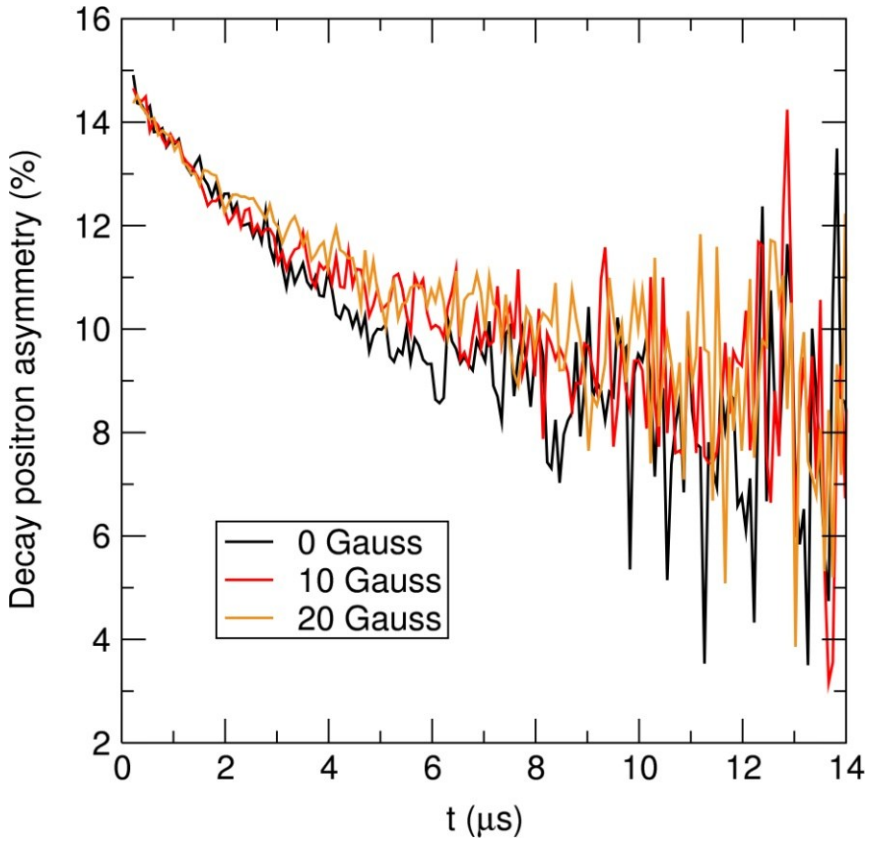


**Figure S14.** Raw $\mu^+$SR data for $LiMnPO_4$ at 300 K at zero field (ZF) and applied longitudinal fields of 10 G and 20 G.

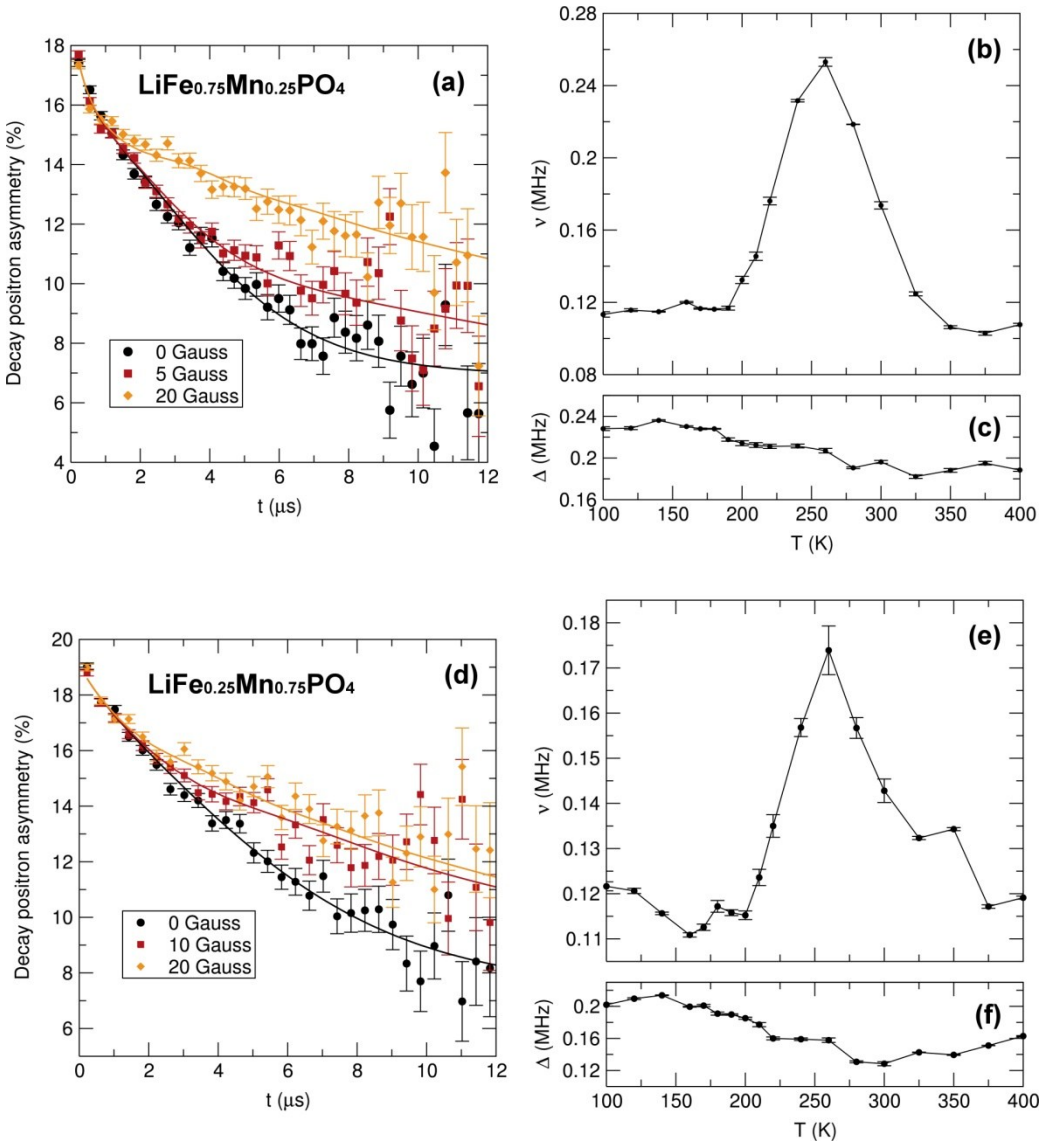


**Figure S15. (a, d)** Raw μ⁺SR data for $LiFe_{0.75}Mn_{0.25}PO_4$ and $LiFe_{0.25}Mn_{0.75}PO_4$ at 300 K at zero field (ZF) [circles] and applied longitudinal fields of 10 G [squares] and 20 G [diamonds], respectively. Temperature dependence of **(b, e)** fluctuation rate ($\nu$) and **(c, f)** field distribution width ($\Delta$) parameters at muon stopping site derived from fitting μ⁺SR data to a dynamic Kubo-Toyabe function for the $LiFe_{0.75}Mn_{0.25}PO_4$ and $LiFe_{0.25}Mn_{0.75}PO_4$) samples, measured from 100 K to 400 K at 0, 10 and 20 G longitudinal fields, respectively.